Connectivity and Entanglement Stress Contributions in Strained Polymer Networks

Carsten Svaneborg,*,† Ralf Everaers,‡ Gary S. Grest,§ and John G. Curro||

Department of Chemistry and Interdisciplinary Nanoscience Center (iNANO), University of Aarhus, Langelandsgade 140, DK-8000 Århus, Denmark, Laboratoire de Physique, École Normale Supérieure de Lyon, CNRS UMR 5672, Université de Lyon, 46 allée d'Italie, 69364 Lyon Cedex 07, France, Sandia National Laboratories, Albuquerque, New Mexico 87185, and Department of Chemical & Nuclear Engineering, University of New Mexico, Albuquerque, New Mexico 87131

Received January 4, 2008; Revised Manuscript Received March 25, 2008

ABSTRACT: Using molecular dynamics simulations and a variant of our primitive path analysis algorithm, we have measured the total stress as well as the connectivity stress contribution for a large variety of generic bead-spring model polymer networks. For randomly cross- and end-linked networks the inferred entanglement stress contribution is excellent agreement with the predictions of the Rubinstein–Panyukov slip-tube model (*Macromolecules* 2002, *35*, 6670). For networks undergoing further cross-linking and bond-breaking in the strained state (chemical aging), the observed stress−strain behavior can be described by a generalization of the slip-tube model in the spirit of Tobolsky's independent network hypothesis. The stress-transfer between independent networks during postcuring appears to obey unexpectedly simple relations.

1. Introduction

Cross-linking a melt of linear chain molecules transforms a viscoelastic liquid into a viscoelastic solid.[1] A piece of rubber can be thought of as a molecule of macroscopic dimensions with memory of its initial shape encoded into its microscopic network structure. The cross-linking process not only creates a random connectivity but also quenches the microscopic topological state of the chain molecules: since the backbones of polymer chains cannot cross, their motion is subject to the same kind of topological constraints one encounters in manipulating knotted strings.[2] Entanglements and cross-links impose qualitatively similar, but subtly different constraints on the conformations of the precursor chains embedded in a network, since entanglents can slip when the network is strained. Due to the presence of two different types of quenched disorder in the system, first principles approaches to the statistical mechanics of rubber elasticity are fraught with difficulties.[3]

The situation is even more complicated for systems undergoing long-term aging and postcuring. Chemical aging involves concomitant changes in the connectivity and topology of the network caused by the formation and breaking of bonds.[4–6] Usually, chemical aging shows effects on significantly longer time scales than the physical relaxation, and determines the changes in elastic properties of polymer networks over years and decades.[7–9] However, in systems containing photosensitive cross-links the effects can be spatially modulated and controlled on a time scale of minutes.[10] While the effect of bond breaking reduces the modulus of the network without affecting its state of ease, the situation is considerably more complex in the case where a strained system undergoes additional cross-linking. In this case, the constitutive behavior of the elastomer depends on the coupling between the cross-linking and strain histories of the network.

Given the inherent complexity of the problem, theories often propose surprisingly simple stress decompositions. Tobolsky and co-workers[4–6] were the first to hypothesize that the constitutive relation for postcured networks could be regarded as the sum of stress contributions from independent networks, each described by the classical stress−strain expression. Each time a batch of cross-links are introduced, an "*independent*" network arises. That independent network has the current deformation as the state-of-ease, and it is characterized by an elastic modulus that depends on the density of cross-links. In the framework of classical rubber elasticity theory, the independent network hypothesis can be proved rigorously.[11,12]

Classical rubber elasticity theory neglects the effects of entanglements. Many statistical mechanical theories try to improve this by including entanglement effects via an additive (and cross-link density independent) term in the constitutive relation.[13–16] Mechanically the summability of the stress corresponds to a sequence of networks coupled in parallel, while teoretically it signifies that the free energy density is a sum of independent contributions. However, there are also counterexamples,[17] and we are not aware of a theoretical argument showing that such a decomposition of stress contributions is rigorously valid.

Computer simulations offer the possibility to identify individual stress contributions.[18,19] This allows us to test the constitutive relations on a deeper level. It is difficult to test the independent network hypothesis having only data for the *total* stress. In the present paper, we use a "*phantom*" variant of our primitive path analysis algorithm[20] to measure the classical stress contribution due to network connectivity for a large variety of model networks which we have studied previously.[21–25] In our earlier work we conjectured that the entanglement contribution to the stress was independent of the postcuring history. In the present work we are able to test this conjecture by inferring the entanglement contribution to the total stress.

While we have devised a way to directly and independently measure a "connectivity contribution to the stress" by investigating the corresponding phantom network, this is not the case for the "entanglement contribution to the stress." The best analogue is probably the plateau regime of the original melt of linear precursor chains, however since additional topological con-

* Corresponding author.
† Department of Chemistry and Interdisciplinary Nanoscience Center (iNANO), University of Aarhus.
‡ Laboratoire de Physique, École Normale Supérieure de Lyon, CNRS UMR 5672, Université de Lyon.
§ Sandia National Laboratories.
|| Department of Chemical & Nuclear Engineering, University of New Mexico.

10.1021/ma800018f CCC: $40.75
Published on Web 06/14/2008

straints are created during cross-linking this procedure is not rigorous. In the following, we will employ the term "entanglement contribution to the stress" for the difference between the total stress and the connectivity contribution. It is clear that this notion has to be taken with due caution, since there are further stress contributions due to e.g. nongaussian chain statistics, chain packing, and thermally excited density fluctuations.[1,26]

The paper is organized as follows: in section 2, we review the theoretical background and introduce our Tobolsky-like generalization of the slip-tube model to account for entanglement effects in chemically aged systems. Model and methods are presented in section 3. In section 4, we present total, connectivity and entanglement stress−strain curves obtained in uniaxial elongation. The extracted moduli and stress transfer between independent networks are discussed in section 5. In section 6, we briefly conclude.

2. Theory

Classical rubber elasticity theory[1] is based on the assumption that the behavior of a polymer network is completely specified by the network connectivity. The theory coarse-grains network strands into entropic springs, and the phantom model[27] integrates out the fluctuations of the remaining degrees of freedom, the positions of the cross-links. In the rest of the paper we will assume an uniaxial volume conserving deformation given by elongation factors $(\lambda, \lambda^{-1/2}, \lambda^{-1/2})$. For linear entropic springs (corresponding to flexible polymers) the elastic response is due to the affine deformation of the mean strand elongations resulting in stress−strain relationships of the form

$$\sigma_c(\lambda;G_c) = G_c[\lambda^2 - \lambda^{-1}] \tag{1}$$

The moduli can be related to the density of strand ν_s as $G_c = \alpha k_B T \nu_s$ with the prefactor $\alpha = 1-2/f$, where f is the functionality of cross-links. In the case of a perfect network with four-functional cross-links $\alpha = 0.5$, and the density of cross-links ν_x is given by $\nu_x = \nu_s/2$, yielding $G_c = k_B T \nu_x$.

The phantom model accounts for stress due to the network connectivity, however, as the name suggests, chains are assumed to be phantom objects that can pass through each other. This is impossible for real molecules—the corresponding topological constraints are often referred to as entanglements. Entanglements are transient in a polymeric melt, and they become quenched and permanent during cross-linking. Cross-links and entanglements are qualitatively similar since both cause the thermal fluctuations of a chain to become localized in space. However, cross-linked monomers are fixed relative to each other, while entanglements can viewed as slip-links which slide along the strands when the network is deformed. Nevertheless, the stress contributions due to the simultaneous presence of cross-links and entanglements are often assumed to be additive. For example, the slip-tube model[16] predicts

$$\sigma(\lambda, G_c, G_e) = \sigma_c(\lambda;G_c) + \sigma_e(\lambda;G_e) \tag{2}$$

with

$$\sigma_e(\lambda;G_e) = \frac{G_e[\lambda^2 - \lambda^{-1}]}{0.74\lambda + 0.61\lambda^{-1/2} - 0.35} \tag{3}$$

here G_e is the modulus of the order of the melt plateau modulus and characterizes the entanglement contribution to the elastic response.

The independent network hypothesis was originally introduced by Tobolsky[5,6] for networks which undergo further cross-linking under strain. For an aged network that has been cross-linked twice, initially in the unstrained state λ_1 (stage 1) and again after elongation to λ_2 (stage 2), Tobolsky postulated a total stress of

$$\sigma_{tot}(\lambda) = \sigma_1(\lambda;\lambda_1 \equiv 1, G_1) + \sigma_2(\lambda;\lambda_2, G_2) \tag{4}$$

The state-of-ease of the resulting network is defined by balance between the tension of the independent stage 1 networks and the compression of the stage 2 network with respect to their respective states-of-ease. The independent network hypothesis has been shown to be exact for the phantom and affine networks models[11,12] where eq 4 takes the form

$$\sigma_c(\lambda;\lambda_2, G_{c,1}, G_{c,2}) = G_{c,1}[\lambda^2 - \lambda^{-1}] + G_{c,2}\left[\left(\frac{\lambda}{\lambda_2}\right)^2 - \left(\frac{\lambda}{\lambda_2}\right)^{-1}\right] \tag{5}$$

In refs 24 and 25 we combined eq 5 with the slip-tube expression in eq 2 for the entanglement stress. A more rigorous implementation of Tobolsky's original idea is to also allow for an entanglement contribution to the σ_2 term in eq 4:

$$\sigma_{tot}(\lambda;\lambda_2, G_{c,1}, G_{c,2}, G_{e,1}, G_{e,2}) = \sigma_c(\lambda;\lambda_2, G_{c,1}, G_{c,2}) + \sigma_e(\lambda;\lambda_2, G_{e,1}, G_{e,2}) \tag{6}$$

with the straightforward generalization

$$\sigma_e(\lambda;\lambda_2, G_{e,1}, G_{e,2}) = \frac{G_{e,1}[\lambda^2 - \lambda^{-1}]}{0.74\lambda + 0.61\lambda^{-1/2} - 0.35} + \frac{G_{e,2}[\lambda^2 {\lambda_2}^{-2} - \lambda^{-1}\lambda_2]}{0.74\lambda {\lambda_2}^{-1} + 0.61\lambda^{-1/2}{\lambda_2}^{1/2} - 0.35} \tag{7}$$

Each stage of cross-linking introduces not one, but two new independent networks—a connectivity and an entanglement network. These independent networks will have different strain dependencies and they will be characterized by different moduli. The various moduli are expected to be nontrivial functions of the postcuring history of a sample. We return to this point in the discussion in section 5 of our simulation results for networks with a variety of postcuring histories.

3. Model and Methods

Our model networks are generated by cross-linking a melt of linear precursor chains. Each chain is represented as a sequence of beads connected by FENE springs, while excluded volume interactions are described by the repulsive part of the Lennard-Jones 12−6 potential (LJ). Cross-links are represented by a FENE spring between a pair of beads on two different chains:

$$U_{FENE}(r) = \frac{k{R_0}^2}{2} \ln\left[1 - \frac{r^2}{{R_0}^2}\right] \quad \text{for } r < R_0$$

$$U_{LJ}(r) = 4\epsilon\left[\left(\frac{\sigma}{r}\right)^{12} - \left(\frac{\sigma}{r}\right)^{6} + \frac{1}{4}\right] \quad \text{for } r < 2^{1/6}\sigma$$

The force field defines the physical units for distance, energy, and time, respectively, as σ, ε, and $\tau = \sigma(m/\varepsilon)^{1/2}$. In our simulations, we used the standard parameters of the Kremer−Grest (KG) force field[28,29] $R_0 = 1.5\sigma$ and $k = 30\varepsilon\sigma^{-2}$. The energy barrier for chain penetration is $\sim 70\varepsilon$, hence ensuring the preservation of the topological state of the network during simulations. The chain dynamics was simulated with the LAMMPS molecular dynamics (MD) code[30] using the Langevin dynamics with time step $\Delta t = 0.012\tau$, friction $\Gamma = 0.5\tau^{-1}$, and temperature $k_B T = 1\varepsilon$. This polymer model maps well on natural rubber.[31] Melts of M chains of length N with bead density $\rho = 0.85\sigma^{-3}$ were generated and equilibrated as described in ref 32.

The precursor melts were cross-linked in two different ways either by end-linking or by random cross-linking. Random-cross-linking[33] is carried out by instantaneously adding FENE bonds between randomly chosen pairs of beads separated by less than the reaction distance of 1.3σ on a precursor melt of 80 chains of 3500 beads. The number of cross-links that is needed to cross the gel-transition is quite low, and we will not attempt to correct cross-

Table 1. Cross-Link Density, Network Connectivity Type End-Linked (E) or Randomly-Cross Linked (R), Average Strand Length, and Connectivity and Entanglement Moduli for Networks

$\nu_1/10^{-4}\ \sigma^{-3}$	type	$\langle N_s \rangle$	$G_c/10^{-4}\ \epsilon\sigma^{-3}$	$G_e/10^{-4}\ \epsilon\sigma^{-3}$
425.0	R	13	366.0	
212.5	R	23	176.7	229.9
42.5	R	101	29.3	142.9
21.3	R	192	14.6	142.3
212.5	E	20	211.0	290.9
121.4	E	35	130.2	191.0
42.5	E	100	38.45	167.9
21.3	E	200	18.81	155.4

link densities to account for those lost before the gel-transition. Melts are end-linked by adding FENE bonds between chain-ends within a reaction radius of 1.3σ from an unsaturated chain end. This process runs until the reaction stops. The resulting networks has less than 7% dangling ends. An important difference between the two cross-linking schemes is that end-linking does not occur instantaneously, since it takes time for chain ends to find each other and react. The resulting stage 1 networks are listed in Table 1.

Previously we characterized and studied the elastic properties of a variety of model networks for a range of deformations,[22,23] in a second set of investigations, we studied the effects of various postcuring histories on the stress[24,25] of randomly cross-linked networks. In these latter investigations the network was elongated by a factor of 2 or 4, and additional cross-links were instantaneously introduced using the same procedure as outlined above for random cross-linking. Typically the stage 2 cross-link density between 0.5 and 1.5 of the stage 1 cross-link density is added. Optionally all the original stage 1 cross-links were removed during this process. These aged model network systems form the basis for the present study. Here we use MD simulations to obtain not only the total stress but also the connectivity stress contributions. This allows us to infer the entanglement contribution to the stress and hence to study its strain dependence as well as as stress-transfer within the independent network hypothesis that we use to describe our data.

In order to obtain the connectivity stress, we determine the ground-state of the corresponding phantom network using a variant of the recently introduced primitive path analysis.[20] FENE springs are replaced by harmonic springs with zero equilibrium extension and spring constant $k_{ppa} = 200\varepsilon\sigma^{-2}$, the simulations are run at $k_B T_{ppa} = 0.001\varepsilon$ with a time step $\Delta t = 0.006\tau$. These simulations differ from the ordinary PPA simulations[20,34–36] by also disabling the interchain excluded volume interactions. Each system is run for at least 1200τ at strain λ_2 to reach mechanical equilibrium after which all network strands are straight. This is computationally trivial compared to solving the equivalent phantom model for the connectivity matrix of our model networks in periodic boundary conditions and allows the analysis of arbitrarily postcured networks. The networks were subsequently compressed in a sequence of steps to $\lambda = 0.25$ or stretched to $\lambda = 5$ at rate of 240τ per strain increment with 1000 MD steps between each successive rescaling of the simulation box dimensions.

The virial stress tensor was sampled continuously, and averaged for each deformation step along an uniaxial deformation pathway. At essentially zero temperature, there are no thermal fluctuations and the deformation is in quasi-equilibrium throughout the entire deformation pathway, hence this procedure provides the strain dependence of the connectivity stress with very good statistics. The stresses obtained from the phantom simulations are obtained from a different force field, and hence different chain statistics, than the regular KG network simulations. In order to directly compare stresses, the phantom simulation stresses σ_{ppa} are mapped as $\sigma_c(\lambda)/k_{KG} = \sigma_{ppa}(\lambda)/k_{ppa}$, where σ_c is the equivalent KG phantom stress. The entropic spring constant is $k_{KG} = 3k_B T/b^2$ with an isotropic Kuhn length $b^2 = 1.7\sigma^2$.[37]

4. Results

4.1. Stage 1 Networks. Figure 1a shows the classical stress contribution $\sigma_c(\lambda)$ for three randomly cross-linked networks. Not surprisingly, the stress−strain relation follows the phantom model prediction eq 1 and allows us to extract the connectivity moduli listed in Table 1. A key result of the present study is shown in the three panels of Figure 2. On the lhs we show the total stresses $\sigma_{tot}(\lambda)$ measured in the MD simulations. The central panel shows that the inferred entanglement stresses, $\sigma_e(\lambda) = \sigma_{tot}(\lambda) - \sigma_c(\lambda)$, of all randomly cross- or end-linked networks. In the panel is also shown the slip-tube expression eq 2 for the entanglement stress contribution. The entanglement modulus should be on the order of the melt plateau modulus. We have used the value $G_e = 0.0145\varepsilon\sigma^{-3}$, which provides a good fit to the data. The melt plateau modulus has been estimated to be in the range of $G_N = 0.0082-0.0105\varepsilon\sigma^{-3}$.[38]

We observe excellent agreement between the slip-tube model and our simulation data of nearly ideal networks. Entanglement stress contributions are observed for all types and degrees of cross-linking with entanglement spacings $\langle N_s \rangle / N_e = 0.2, ..., 3.1$ using the entanglement length $N_e = 65 \pm 7$.[20] To extract the entanglement moduli, we fitted $\sigma_e(\lambda; G_e)$ to the sampled $\sigma_{tot} - \sigma_c$ within the range of $1 \le \lambda \le 2$ for each system. Good fits were obtained for all systems. Deviations are observed to occur at larger deformations only, which we attribute to finite chain length effects, as they are most pronounced for the systems with short strands.

4.2. Aged Networks. Figure 1b shows the classical stress contribution $\sigma_c(\lambda)$ for three aged networks derived from the same stage 1 network by additional cross-linking at a strain of $\lambda_2 = 2$. The data are in excellent agreement with the Tobolsky form in eq 5. Figure 1c shows the corresponding curves for the same networks after removal of the original stage 1 cross-links. Again, the data are in excellent agreement with the Tobolsky form. The fact that their state-of-ease has not shifted to λ_2 indicates the presence of *stress transfer*[4] between the independent networks. Values for the extracted connectivity moduli are listed in Table 2.

In Figure 3, we show again the total stresses $\sigma_{tot}(\lambda)$ measured in the MD simulations and the inferred entanglement stresses, $\sigma_e(\lambda) = \sigma_{tot}(\lambda) - \sigma_c(\lambda)$. The latter no longer collapse to the simple slip-tube prediction as they did in Figure 2b for networks cross-linked once. The entanglement stress contribution also displays a permanent set. To extract the entanglement moduli, we again fitted $\sigma_e(\lambda; \lambda_2, G_{e,1}, G_{e,2})$ to the sampled $\sigma_{tot} - \sigma_c$ within the range of $1 \le \lambda \le 2$ for each system. Good fits were obtained for all systems. Up to finite-chain length effects, the data are in excellent agreement with our Tobolsky-like generalization of eqs 6 and 7 of the RP expression. Values for the extracted entanglement moduli are listed in Table 2.

5. Discussion

The stress residuals in Figures 2c and 3c demonstrate the excellent agreement between the sampled stresses and the slip-tube model with respect to its Tobolsky-like generalization in eq 6. In the following, we take a closer look at the extracted moduli and their relation to the postcuring history.

5.1. Stage 1 Networks. The symbols in Figure 4 show the classical and entanglement moduli we extracted for the networks after the initial cross-linking of the equilibrated precursor chain melt. In agreement with classical rubber elasticity theory, $G_c = 2\alpha k_B T \nu_1$. The phantom model predicts that $\alpha = 0.5$ for a perfect 4-functional network. From our simulations we obtain $\alpha = 0.42$, which is consistent with the phantom model, when taking into account that about 85% of the strands are elastically active. The rest are network defects such as dangling-ends or self-loops that do not contribute to the modulus in a phantom simulation.

The modulus of the end-linked networks with short strands are observed to be above that of the randomly cross-linked

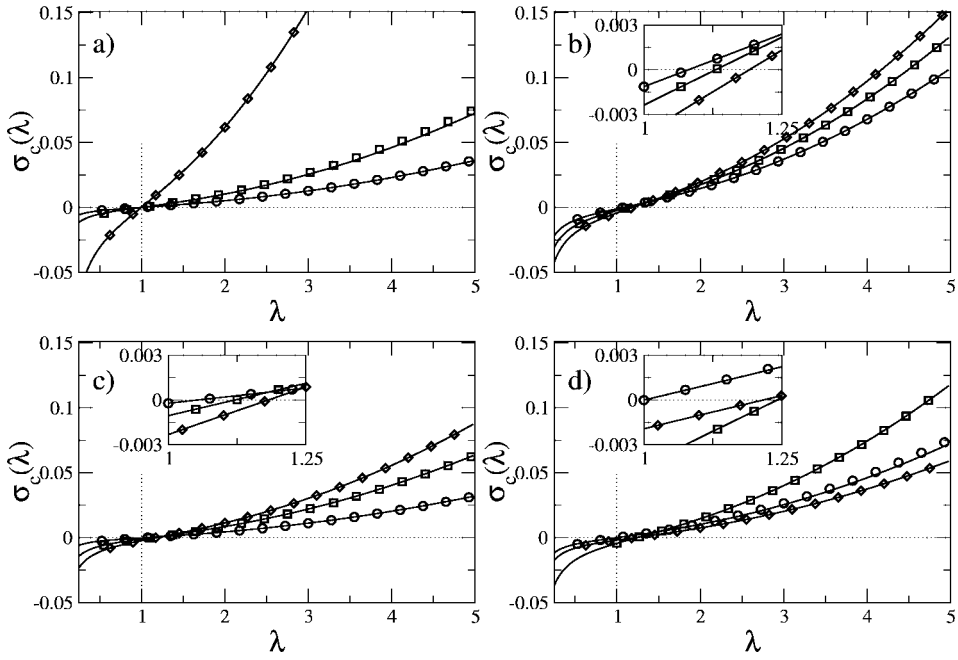

Figure 1. Connectivity stress−strain relationship for randomly cross-linked networks. Key: (a) stage 1 networks with $\nu_1 = 21.3, 42.5, 212.5 \times 10^{-4}\sigma^{-3}$ (○, □, ◇); (b) stage 1 network with $\nu_1 = 42.5 \times 10^{-4}\sigma^{-3}$ elongated to $\lambda_2 = 2.0$ and postcured with a cross-link density of $\nu_2 = 0.5\nu_1$, ν_1, or $1.5\nu_1$ (○, □, ◇ respectively); (c) networks in part b after the removal of all stage 1 cross-links; (d) postcuring history on a particular stage 1 network with $\nu_1 = 42.5 \times 10^{-4}\sigma^{-3}$ cross-links (○), elongated to $\lambda_2 = 4.0$ and postcured with a $\nu_2 = \nu_1$ cross-link density (□), and after removal of the original stage 1 cross-links (◇). The black lines are the classical stress−strain behavior (a) or eq 5 (b−d). The insets show a blow up of the stress−strain behavior around the state-of-ease.

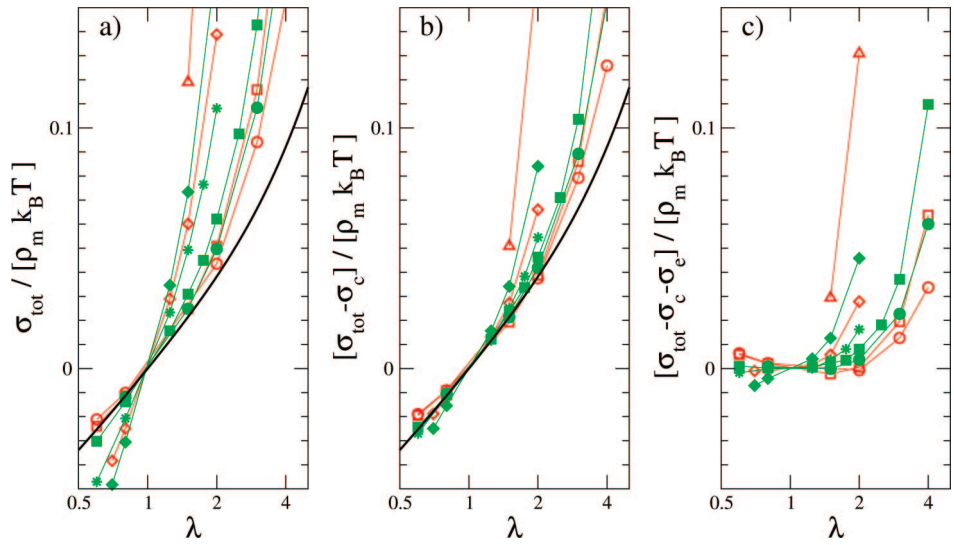

Figure 2. Total network stress (left), total stress with the connectivity stress contribution subtracted (center), and residual stress when subtracting both connectivity and entanglement stress contributions. Symbols denote randomly cross-linked networks with $\nu_1 = 21.3, 42.5, 212.5, 425 \times 10^{-4}\sigma^{-3}$ (red filled ○, □, ◇, Δ), end-linked networks with $\nu_1 = 21.3, 42.5, 121.4, 212.5 \times 10^{-4}\sigma^{-3}$ (green open ○, □, ∗, ◇) . Shown is also the slip-tube models prediction for the entanglement stress $\sigma_e(\lambda; G_e = 0.0145\varepsilon\sigma^{-3})$ (solid line).

networks, which could be due to chain deformations introduced by the cross-linking process. The randomly cross-linked networks are instantaneously cross-linked as are the stage 2 cross-links. The extracted entanglement moduli for the networks with long strands are observed to be in very good agreement with the melt plateau modulus, but deviate for shorter strands, which is an artifact of our fitting procedure which use data from a fixed range of deformations and hence is affected differently by finite chain length effects. These observations strongly support the slip-tube model.

5.2. Aged Networks. Can we rationalize, the changes resulting from the addition or removal of cross-links under strain? The first case is subject to an important constraint: the instantaneous addition of cross-links does not change the stress. In general, static network observables do not change due to cross-link constraints as long as the networks is not strained. The probability of particular realization of instantaneous cross-linking is proportional to the Boltzmann factor for the occurrence of that precursor state. That Boltzmann factor for the occurrence of the precursor state is retrieved when making a thermal average

Table 2. Aged Networks with Two Stages of Cross-Linking[a]

$\nu_1^*/10^{-4}\ \sigma^{-3}$	λ_2	$\nu_1/10^{-4}\ \sigma^{-3}$	$\nu_2/10^{-4}\ \sigma^{-3}$	$\langle N_s \rangle$	$G_{c,1}/10^{-4}\ \epsilon\sigma^{-3}$	$G_{c,2}/10^{-4}\ \epsilon\sigma^{-3}$	$G_{e,1}/10^{-4}\ \epsilon\sigma^{-3}$	$G_{e,2}/10^{-4}\ \epsilon\sigma^{-3}$
42.5	2	42.5	21.3	69	41.7	6.5	125.0	40.3
42.5	2	42.5	42.5	53	50.1	13.5	100.2	33.2
42.5	2	42.5	63.8	43	56.3	24.6	99.1	42.9
42.5	4	42.5	21.3	69	41.0	4.5	121.9	19.2
42.5	4	42.5	42.5	53	47.3	11.2	108.0	28.9
42.5	4	42.5	63.8	43	51.5	21.1	100.4	42.7
42.5	2	0	21.3	193	12.7	1.2	114.0	27.5
42.5	2	0	42.5	100	24.3	6.0	104.3	34.5
42.5	2	0	63.8	69	32.4	13.3	97.3	41.9
42.5	4	0	42.5	101	23.8	4.9	100.2	27.3
85.0	2	0	42.5	101	25.6	5.4	110.3	28.0
85.0	2	0	85.0	52	43.6	20.0	98.6	42.5

[a] Columns are density of cross-links introduced in stage 1, elongation factor, density stage 1 of cross-links remaining, and density of stage 2 cross-links introduced, average strand length, connectivity moduli for stage 1 and 2 networks, entanglement moduli for stage 1 and 2 networks, respectively.

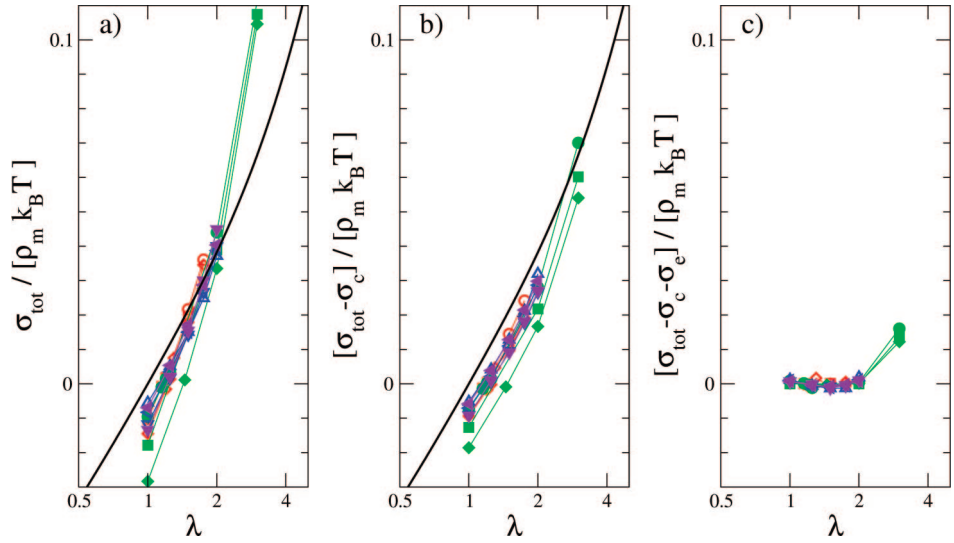

Figure 3. Total network stress (left), total stress with the connectivity stress contribution subtracted (center), and residual stress when subtracting both connectivity and entanglement stress contributions for aged networks. Symbols denote randomly cross-linked systems with $\nu_1 = 42.5 \times 10^{-4}\sigma^{-3}$ cross-links strained to $\lambda_2 = 2$ or 4 (red open and green filled symbols, respectively) and stage 2 cross-linked with $\nu_2 = 0.5\nu_1, \nu_1, 1.5\nu_1$ (○, □, ◇). Also shown are networks with $\nu_1 = 42.5, 85 \times 10^{-4}\sigma^{-3}$ stage 1 cross-links (blue open, violet filled) strained to $\lambda_2 = 2$ where the original cross-links were instantaneously removed and $\nu_2 = 0.5\nu_1^{\dagger}, \nu_1^{\dagger}, 1.5\nu_1^{\dagger}$ new stage 2 cross-links introduced (triangle up, left, down, respectively). The line denotes the slip-tube models prediction for entanglement stress σ_e (λ; $G_e = 0.0145\varepsilon\sigma^{-3}$) .

for a given set of cross-links and subsequently averaging over cross-link realizations.[3] For systems sufficiently large to be self-averaging the second (quenched-variable) average is automatically carried out. Hence the presence of further cross-links is only felt after further deformation.

If we consider eq 6 from this point of view, it is obvious that the two newly formed independent networks fulfill this condition, because they have the current strain as the state of ease. For those independent networks which existed previously, only the sum of the stresses has to be conserved, but the individual contributions are free to change. There is thus the possibility of a *stress transfer* between independent networks equivalent to a change of the respective elastic moduli during aging. Stress transfer will also occur in the case where cross-links introduced in previous stages are removed, however the total stress will not be conserved in this case.

In Figure 5, we show the four extracted moduli for each aged networks as function of density of cross-links added under strain, ν_2. $G_{c,2}$ is seen to increase as expected, concomitantly $G_{e,2}$ increases as the new cross-links trap entanglements in the strained state. $G_{e,1}$ is also observed to decrease while $G_{c,1}$ increases; thus stage 2 cross-linking has the effect of converting stage 1 entanglements into stage 1 cross-links. This observation can be rationalized from the constraint that the total stress has to be constant. By construction, the two independent stage 2 networks does not contribute any stress in their state-of-ease. The total stress is thus distributed between the stage 1 entanglement and connectivity networks, and it has to remain constant. As a result, the respective moduli are anticorrelated. It is instructive to compare this to the case of classical rubber elasticity theory, which neglects the stress contribution due to entanglements. In this case, the only stress contribution is from the stage 1 connectivity network, and the corresponding modulus can not change during stage 2 cross-linking.

The moduli for aged networks where the stage 1 cross-links were completely removed are shown in Figure 6. We observe the same qualitative results as for the networks where the stage 1 cross-links were kept. It is interesting to note that removing the stage 1 cross-links does not have to lead to the vanishing of the corresponding modulus. The stage 2 cross-links were introduced in a strained state of the network with stage 1 cross-links present, and hence it retains a memory of their effect on the network. Removing stage 1 cross-links is observed to lower both the stage 1 and 2 connectivity moduli, and the stage 1 connectivity moduli extrapolate to zero as expected. It is interesting to note that the stage 2 connectivity moduli for both aging protocols shown in Figure 5 and 6 appears to extrapolate to a negative value for $\nu_2 \rightarrow 0$, suggesting the presense of a gel-point of the stage 2 network, that has to be crossed.

From Figure 7, we can see that the sum of the connectivity moduli is proportional to the sum of the cross-link densities, while within the precision of our data the sum of entanglement

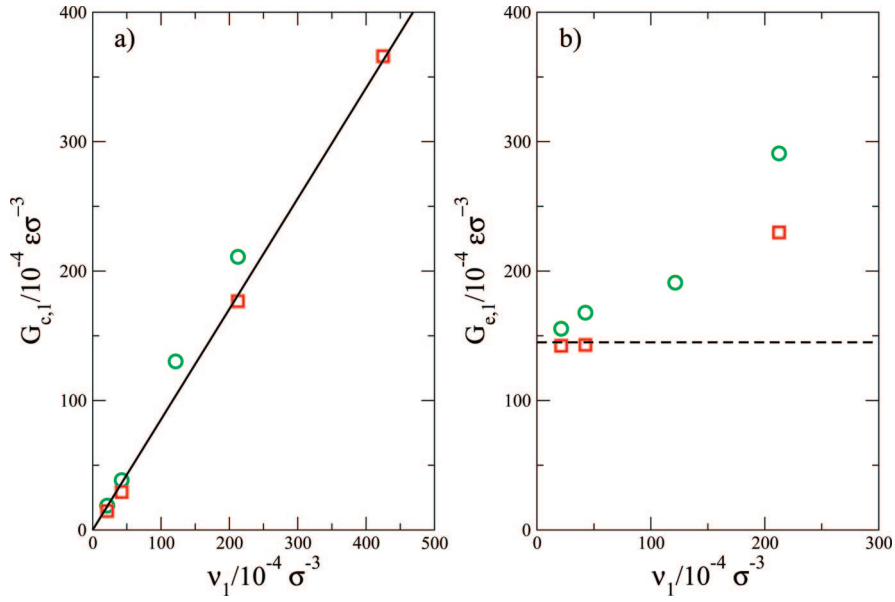

Figure 4. Connectivity (left) and entanglement (right) moduli for stage 1 networks. Symbols denote end-linked and randomly cross-linked networks (green ○, red □, respectively). The solid straight line corresponds to $\alpha = 0.42$.

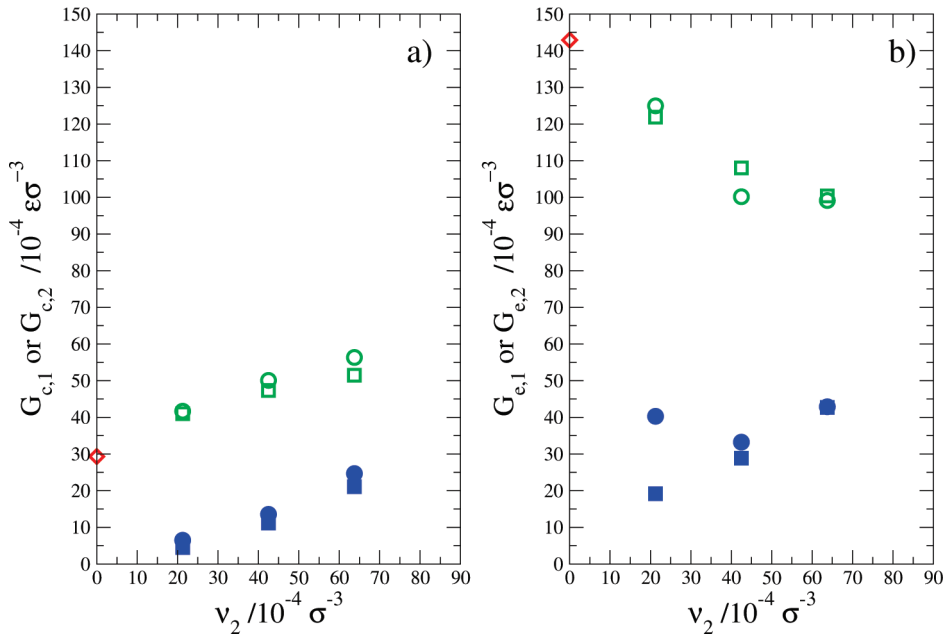

Figure 5. Moduli vs density of added stage two cross-links. Symbols denote $G_{c,1}$ or $G_{e,1}$ (open green symbols) and $G_{c,2}$ or $G_{e,2}$ (filled blue symbols) for networks with $\nu_1 = 42.5 \times 10^{-4}\sigma^{-3}$ and $\lambda_2 = 2$ (○), $\lambda_2 = 4$ (□). Also shown is the moduli for the corresponding stage 1 network (red ◇).

moduli is independent of both ν_1 and ν_2. On the basis of these observations, we attempt to rationalize the behavior in terms of a stress-transfer function Φ_c with the simplest possible relation:

$$G_{c,1}(\nu_1, \nu_2) = G^{T}_{c,1}(\nu_1) + \Phi_c G^{T}_{c,2}(\nu_2)$$
$$G_{c,2}(\nu_1, \nu_2) = (1 - \Phi_c) G^{T}_{c,2}(\nu_2) \qquad (8)$$

where superscript "T" is used to distinguish between the observed moduli and theoretical moduli given by $G^{T}_{c}(\nu_x) = 2\alpha k_B T \nu_x$ where ν_x is the density of cross-links. In figure 5 the effective moduli are shown as function of the density of stage 2 cross-links, the linear behavior observed in the figure qualitatively confirms the stress-transfer picture. In the stress-transfer picture it is assumed that the number of effective cross-links is conserved, hence the sum of the effective moduli is $G_{c,1} + G_{c,2} = G^{T}_{c,1} + G^{T}_{c,2} = 2\alpha k_B T(\nu_1 + \nu_2)$. In Figure 7, we plot these two sums, and very good agreement with the theoretical expectation is observed, confirming the conservation of the number of cross-links.

Having access to the two entanglement moduli, we are now able to study how aging affects stage 1 and 2 entanglements. Figure 6 shows that stage 1 entanglements decrease, while stage 2 entanglements increase as the system undergoes further cross-linking. This indicates a stress-transfer from stage 1 entanglements to stage 2 entanglements. The sum of the stage 1 and 2 entanglement moduli is shown in Figure 7. We see that the sum of the entanglement moduli is independent of the density of stage 2 cross-links and the strain state in which they were introduced, hence the number of entanglements per strand is conserved during postcuring. Similar to the connectivity moduli,

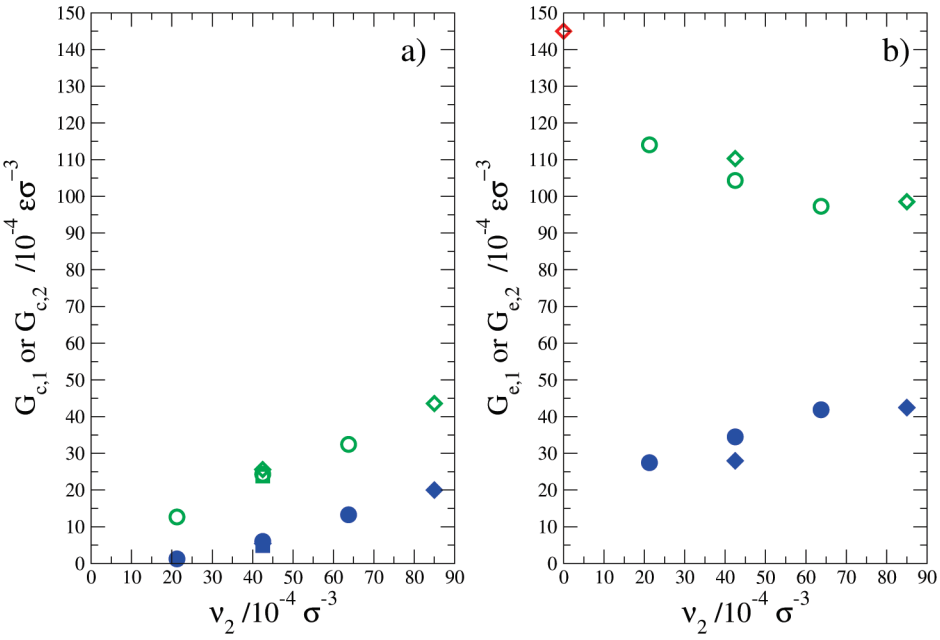

Figure 6. Moduli vs density of stage two cross-links for networks where the stage 1 cross-links were removed. Symbols denote $G_{c,1}$ or $G_{e,1}$ (open green symbols) and $G_{c,2}$ or $G_{e,2}$ (filled blue symbols) for networks with $\nu_1^* = 42.5 \times 10^{-4}\sigma^{-3}$ and $\lambda_2 = 2$ (○), $\lambda_2 = 4$ (□), or $\nu_1^* = 85.0 \times 10^{-4}\sigma^{-3}$ and $\lambda_2 = 2$ (◇) . Also shown is the melt plateau modulus (red ◇).

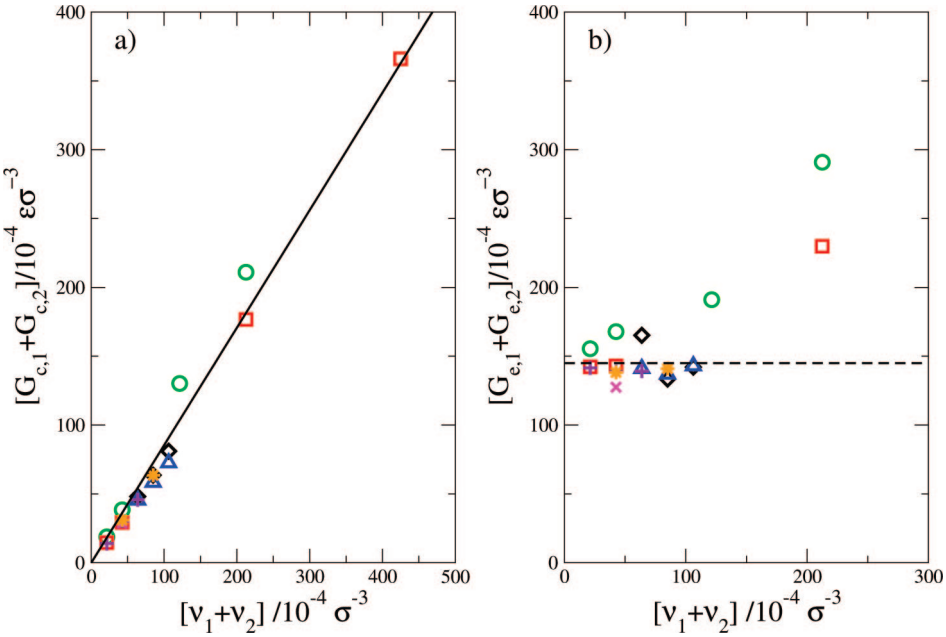

Figure 7. Sum of connectivity (left) and entanglement (right) moduli for all networks vs the total cross-link density. Symbols denote end-linked and randomly cross-linked networks (green ○ and red □, respectively), aged networks with $\nu_1 = 42.5 \times 10^{-4}\sigma^{-3}$ strained to $\lambda_2 = 2$ or 4 (black ◇, blue Δ) and further cross-linked. Also shown are networks with $\nu_1^* = 42.5 \times 10^{-4}\sigma^{-3}$ strained to $\lambda_2 = 2$ or 4 and further cross-linked while original cross-links were removed (violet +, magenta ×), similar networks with $\nu_1^* = 85 \times 10^{-4}\sigma^{-3}$ strained to $\lambda_2 = 2$ (orange ∗).

we can attempt to relate the two entanglement moduli by introducing an entanglement stress-transfer function Φ_e as

$$G_{e,1}(\nu_1, \nu_2) = G_N - \Phi_e G^T_{e,2}(\nu_2)$$
$$G_{e,2}(\nu_1, \nu_2) = \Phi_e G^T_{e,2}(\nu_2) \quad (9)$$

where according to the slip-tube model $G^T_{e,i}(\nu) = (8/7)\nu_x k_B T L$ where L is the number of slip-links per network strand, and ν_x the density of cross-links.[16] Using $G_N = 0.0145\varepsilon\sigma^{-3}$ yields $L/\langle N_s\rangle = 0.03$ which corresponds to a slip-link spacing of 33.5 beads, which is half of the entanglement length $N_e = 65$ as obtained from a primitive path analysis.[20]

We have introduced the two stress-transfer functions Φ_c and Φ_e, but are they related? From the two equations for the connectivity stress-transfer in eq 8, we obtain two values for the connectivity stress-transfer function for each system. They differ slightly due to statistical uncertainties, but provide an average value $\langle\Phi_c\rangle$. We can obtain a similar estimate for the entanglement stress-transfer function from eq 9. The results are plotted in Figure 8, and show a clear anticorrelation suggesting the surprisingly simple relation between the connectivity and entanglement stress transfer functions: $\Phi_c(\nu_1, \nu_2; \lambda_2) = 1 - \Phi_e(\nu_1, \nu_2; \lambda_2)$.

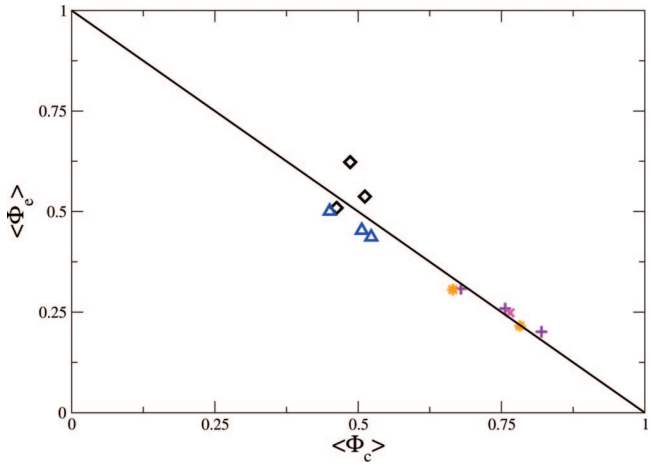

Figure 8. Connectivity stress-transfer function vs entanglement stress transfer function. Aged networks with $\nu_1 = 42.5 \times 10^{-4}\sigma^{-3}$ strained to $\lambda_2 = 2$ or 4 (black ◇, blue Δ) and further cross-linked, networks with $\nu_\uparrow = 42.5 \times 10^{-4}\sigma^{-3}$ strained to $\lambda_2 = 2$ or 4 and further cross-linked while original cross-links were removed (violet +, magenta ×) and similar networks with $\nu_\uparrow = 85 \times 10^{-4}\sigma^{-3}$ strained to $\lambda_2 = 2$ (orange ∗).

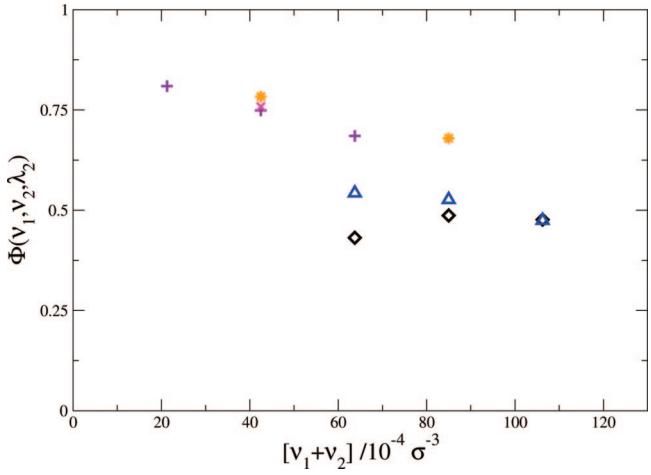

Figure 9. Average stress-transfer as function of total density of cross-links. Symbols are as in Figure 8.

Having now reduced the entire postcuring history of a network to a single number given by the (average) stress-transfer $\Phi = (\langle\Phi_c\rangle + [1 - \langle\Phi_e\rangle])/2$, we can summarize the results for instance by plotting them as function of the total density of cross-links as is done in Figure 9. We observe a stronger stress-transfer for the systems where the initial stage 1 cross-links were completely removed compared to the networks where they were retained. The stress-transfer is also observed to decreases as the density of stage 2 cross-links is increased. For both models of aging and different aging histories, we observe an approximate collapse of the data points as function of the total density of cross-links, suggesting that this is a relevant parameter for understanding the change of elastic properties of these networks with aging.

6. Conclusion

We have studied connectivity and entanglement stress contributions for a large variety of strained model polymer networks, some of which have a complex postcuring history. While standard molecular dynamics simulations provide access to the *total* elastic response, we have introduced a variant of our primitive path analysis[20] which implements a frequently employed Gedankenexperiment that allows us to measure the *connectivity* contribution to the total stress from the elastic response of the corresponding phantom networks. We are thus in a position to quantitatively explore the pertinence of the decomposition of network stresses in additive and independent connectivity and entanglement contributions.

In the case of randomly cross and end-linked model networks, the connectivity contributions to the stress are in excellent agreement with classical rubber elasticity theory. Most remarkably, the inferred entanglement stress contributions collapse to a single curve in very good agreement with the functional form predicted by the slip-tube model,[16] for a value of the entanglement modulus which closely agrees with the plateau modulus obtained in previous simulations for the corresponding long chain linear melts.[29]

We have also investigated the considerably more complex situation of chemical aging under strain. In this case, the measured connectivity stress contributions are in excellent agreement with Tobolsky's independent network hypothesis,[4] where each stage of cross-linking sets up an independent network with the current strain state as the state-of-ease. In a second step, we found that the inferred entanglement stresses exhibit a permanent set. This can be account for by our generalization in eq 6 of the Tobolsky construction: each cross-linking stage introduces *two* additional independent networks, one representing connectivity and a second representing trapped entanglements.

We have used the slip-tube[16] expression for the entanglement stress contribution and determined the corresponding moduli by fitting the inferred entanglement stress contributions from our simulation results. Interestingly, the extracted moduli seem to follow surprisingly simple relations. In particular, the sum of the connectivity moduli seems to be related to the total cross-link density and the sum of the entanglement moduli appears to be a constant of the order of the melt plateau modulus. In contrast, the variation of individual moduli (stress transfer) with the addition and removal of cross-links under strain is highly nontrivial.

It is important to emphasize that while we use these independent networks and the concept of stress-transfer to rationalize the effects of aging on the stress−strain response of our networks, actually attempting to imbue these concepts with a microscopic interpretation is very difficult. We exactly know which cross-links were introduced during stage 1 or 2 cross-linking of our networks. However, the stresses we obtain are caused by the localization of the thermal fluctuations of network strands. This localization is due to the confinement caused by the other chains in the neighborhood of the strand either directly via cross-linkers or entanglements or indirectly via entanglements and cross-links between the neighboring chains themselves. Attempting to assign a given network strand from our simulation to one of the independent networks is very likely to fail given the complex interplay between these effects, aging, and the deformation history on microscopic network conformations.

To summarize, we have used simulation techniques to carry out a Gedankenexperiment: the separation of the total elastic response of (chemically aged) polymer networks into a connectivity and an entanglement contribution. While we do not mean to imply that the independent network hypothesis and (our generalization of) the slip-tube model are exact, their remarkable success is of practical interest, and calls for a theoretical explanation. These insights might suggest a way to make the highly complex problem of the statistical mechanics of (aging) polymer networks under strain more tractable.

Acknowledgment. C.S. gratefully acknowledges financial support from the Danish Natural Sciences Research Council through

a Steno Research Assistant Professor fellowship. R.E. is supported by a chair of excellence grant from the Agence Nationale de Recherche (France). Sandia is a multiprogram laboratory operated by Sandia Corporation, a Lockheed Martin Company, for the U.S. Department of Energy under Contract No. DE-AC04-94AL85000.

References and Notes

(1) Treloar, L. R. G. *The Physics of Rubber Elasticity*; Clarendon: Oxford, U.K., 1975.
(2) Edwards, S. F. *Proc. Phys. Soc.* **1967**, *92*, 9.
(3) Deam, R. T.; Edwards, S. F. *Phil. Trans. R. Soc. London, A* **1976**, *280*, 317.
(4) Tobolsky, A. V. *Properties and Structure of Polymers*; Wiley: New York, 1960.
(5) Tobolsky, A. V.; Prettyman, I. B.; Dillon, J. H. *J. Appl. Phys.* **1944**, *15*, 380.
(6) Andrews, R. D.; Tobolsky, A. V.; Hanson, E. E. *J. Appl. Phys.* **1946**, *17*, 352.
(7) Curro, J. G.; Salazar, E. A. *J. Appl. Polym. Sci.* **1975**, *19*, 2571.
(8) Curro, J. G.; Salazar, E. A. *Rubber Chem. Technol.* **1977**, *50*, 895.
(9) Salazar, E. A.; Curro, J. G.; Gillen, K. T. *J. Appl. Polym. Sci.* **1977**, *21*, 1597.
(10) Scott, T. F.; Schneider, A. D.; Cook, W. D.; Bowman, C. N. *Science* **2005**, *308*, 1615.
(11) Flory, P. J. *Trans. Faraday. Soc.* **1960**, *56*, 722.
(12) Fricker, H. S. *Proc. R. Soc. London A* **1973**, *335*, 269.
(13) Langley, N. R. *Macromolecules* **1968**, *1*, 348.
(14) Frank-Kamenetskii, M. D.; Lukashin, A. V.; Vologodskii, A. V. *Nature* **1975**, *258*, 398.
(15) Everaers, R.; Kremer, K. *Phys. Rev. E* **1996**, *53*, R37.
(16) Rubinstein, M.; Panyukov, S. *Macromolecules* **2002**, *35*, 6670.
(17) Mergell, B.; Everaers, R. *Macromolecules* **2001**, *34*, 5675.
(18) Everaers, R.; Kremer, K. *Macromolecules* **1995**, *28*, 7291.
(19) Everaers, R. *New J. Phys.* **1999**, *1*, 12–1.
(20) Everaers, R.; Sukumaran, S. K.; Grest, G. S.; Svaneborg, C.; Sivasubramanian, A.; Kremer, K. *Science* **2004**, *303*, 823.
(21) Rottach, D. R.; Curro, J. G.; Grest, G. S.; Thompson, A. P. *Macromolecules* **2004**, *37*, 5468.
(22) Svaneborg, C.; Grest, G. S.; Everaers, R. *Phys. Rev. Lett.* **2004**, *93*, 257801.
(23) Svaneborg, C.; Grest, G. S.; Everaers, R. *Polymer* **2005**, *46*, 4283.
(24) Rottach, D. R.; Curro, J. G.; Budzien, J.; Grest, G. S.; Svaneborg, C.; Everaers, R. *Macromolecules* **2006**, *39*, 5521.
(25) Rottach, D. R.; Curro, J. G.; Budzien, J.; Grest, G. S.; Svaneborg, C.; Everaers, R. *Macromolecules* **2007**, *40*, 131.
(26) Xing, X.; Goldbart, P. M.; Radzihovsky, L. *Phys. Rev. Lett.* **2007**, *98*, 075502.
(27) James, H. *J. Chem. Phys.* **1943**, *15*, 651.
(28) Grest, G. S.; Kremer, K. *Phys. Rev. A* **1986**, *33*, 3628.
(29) Kremer, K.; Grest, G. S. *J. Chem. Phys.* **1990**, *92*, 5057.
(30) Plimpton, S. J. Large-scale Atomic/Molecular Massively Parallel Simulatorhttp://lammps.sandia.gov.
(31) Sukumaran, S. K.; Grest, G. S.; Kremer, K.; Everaers, R. *J. Polym. Sci., Part B: Polym. Phys.* **2005**, *43*, 917.
(32) Auhl, R.; Everaers, R.; Grest, G. S.; Kremer, K.; Plimpton, S. J. *J. Chem. Phys.* **2003**, *119*, 12718.
(33) Grest, G. S.; Kremer, K. *Macromolecules* **1990**, *23*, 4994.
(34) Zhou, Q.; Larson, R. G. *Macromolecules* **2005**, *38*, 5761.
(35) Kröger, M. *Comput. Phys. Commun.* **2005**, *168*, 209–232.
(36) Tzoumanekas, C.; Theodorou, D. *Macromolecules* **2006**, *39*, 4592–4604.
(37) Duering, E. R.; Kremer, K.; Grest, G. S. *J. Chem. Phys.* **1994**, *101*, 8169.
(38) Pütz, M.; Kremer, K.; Grest, G. S. *Europhys. Lett.* **2000**, *49*, 735.

MA800018F